Solar Light-Driven Photocatalytic Degradation of Methylene Blue by Mesoporous g-C_3N_4@BiOCl hybrid

A thesis

submitted in the partial fulfilment of the requirements for the degree of

MASTER OF SCIENCE

IN

CHEMISTRY

Submitted by

AAYUSHI

(Roll No. 301702002)

Under the supervision of

Dr. SOUMEN BASU

(Associate Professor)

School of Chemistry and Biochemistry

Thapar Institute of Engineering & Technology, Patiala

July-2019

CERTIFICATE

I hereby declare that the thesis entitled **"Solar Light-Driven Photocatalytic Degradation of Methylene Blue by Mesoporous g-C_3N_4@BiOCl hybrid."** is an authentic record of my work carried out as requirements for the award of the degree of Master of Science in Chemistry at Thapar Institute of Engineering and Technology, Patiala under the supervision of Dr. Soumen Basu, Associate Professor, School of Chemistry & Biochemistry, Thapar Institute of Engineering and Technology, Patiala during July' 2017 to July' 2019. No part of the matter embodied in this report has been submitted to any other university or institute for the award of any degree.

Aayushi

Aayushi

Date: 12/07/2019

It is certified that the above statement made by the student is correct to the best of my knowledge and belief.

Basu

Dr. Soumen Basu

Associate Professor,

School of Chemistry & Biochemistry

Thapar Institute of Engineering and Technology, Patiala - 147004

ACKNOWLEDGEMENT

First of all, I owe my gratitude to the Head of the Department, **Dr. Amjad Ali** for providing me an opportunity in the form of this dissertation to develop my interest in research.

In the same spirit, I would like to thank my Supervisor, **Dr. Soumen Basu** for his constructive guidance and constant support during the project. The work presented here could not have been accomplished without his patience and ever willingness to teach. He has taught me to be concise and correct in my approach from the formulation of ideas to the presentation of the results.

I would also like to express my gratitude to **Ms. Surbhi Sharma, Ms. Aanchal Rathi, Ms. Neeraj, Ms. Shagun, Ms. Divya and Mr. Jasminder Singh** who never turned me down whenever I approached them for any kind of help.

I am grateful to **Thapar Institute of Engineering and Technology & School of Chemistry and Biochemistry** for providing financial support and all necessary infrastructure and laboratory facilities to carry out the experimental work.

I fall short of words to express my thanks to my Parents, younger brother **Aditya** and friends who have always supported me and have been a source of strength and inspiration to me during the entire period of my work.

All these thanks are, however, only fraction of what is due to almighty for granting me an opportunity and strength to successfully accomplish this project.

Aayushi

Aayushi

Dedicated To My Family

ABSTRACT

Photocatalytic degradation of noxious pollutants has emerged as the most appealing technique to minimize water pollution. Here a facile approach has been developed for the construction of g-C_3N_4@BiOCl hybrid with varying weight ratios by the conglomeration of g-C_3N_4 nanosheets with BiOCl in-situ. The successful formation, uniform distribution and thermal stability of the hybrid were verified by XRD, XPS, EDX, elemental mapping and TGA analysis. FESEM and HRTEM images displayed that BiOCl platelets are well-covered with g-C_3N_4 nanosheets. The optical properties were evaluated by UV-DRS and PL spectroscopy which confirmed that the hybrid has a low band gap and low recombination rate, facilitating charge-separation. BET analysis revealed that 3:1 g-C_3N_4@BiOCl had the highest surface area (107m^2/g) with mesopores. To evaluate the photocatalytic performance of the catalyst, methylene blue (MB) was degraded in natural sunlight. The 3:1 g-C_3N_4@BiOCl hybrid manifested the best performance (degrading 94.8% of MB with very high rate constant (0.0301 min^{-1}). Effect of pH and catalyst concentration on the photodegradation was also investigated. Trapping experiments revealed that $O_2^{\bullet-}$ was the major reactive species in the photodegradation mechanism. The catalyst was reused for MB degradation showing 76% efficiency even after 5 consecutive-cycles. A comparative study was done with catalysts in the literature suggesting that the synthesized nanocomposite acts as one of the best photocatalyst for degradation of hazardous contaminants.

CONTENTS

LIST OF FIGURES

LIST OF SCHEMES

TABLES

LIST OF ABBREVIATIONS AND SYMBOLS

1.	**BOD**	Biological Oxygen Demand
2.	**BET**	Brunauer-Emmett-Teller
3.	**RhB**	Rhodamine B
4.	**AOPs**	Advanced Oxidation Processes
5.	**eV**	Electron Volt
6.	**Nm**	Nanometer
7.	**^oC**	Degree Celsius
8.	**g-C_3N_4**	Graphitic Carbon Nitride
9.	**UTI**	Urinary tract Infection
10.	**MB**	Methylene Blue
11.	**MO**	Methyl Orange
12.	**EDX/EDS**	Energy dispersive X-ray spectroscopy
13.	**Ɵ**	Theta
14.	**Min**	Minutes
15.	**M**	Molar

16.	**N**	Normal
17.	**H**	Hours
18.	**G**	Gram
19.	**Λ**	Wavelength
20.	**λ_{max}**	Maximum wavelength
21.	**K**	Kelvin
22.	**m^2g^{-l}**	Meter square per gram
23.	**Mm**	Micrometer
24.	**µL**	Micro litre
25.	**Ppm**	Parts per million
26.	**mL**	Millilitre
27.	**MW**	Molecular Weight
28.	**NS**	Nanosheets
29.	**%**	Percentage
30.	**BJH**	Barrett– Joyner–Halenda
31.	**kV**	KiloVolt
32.	**FESEM**	Field Emission Scanning electron microscope
33.	**Mg**	Miligram
34.	**UV-Vis**	Ultraviolet-Visible
35.	**W**	Watt
36.	**XRD**	X-ray diffractometer
37.	**XPS**	X-ray photoelectron spectroscopy
38.	**a.u.**	Arbitrary Units

CHAPTER 1: INTRODUCTION

Water pollution has become a fatal threat to macrocosm by affecting mankind, aquatic life, and ecological environment dangerously [1]. Increasing industrialization and rapid globalization are the major causes of water pollution [2]. The discharge of huge amounts of water pollutants like organic dyes [3], phenol [4], polymers, benzene based organics [5] and other perilous chemicals in natural water resources are a hazard to living beings as these are highly toxic, carcinogenic and hard to degrade [6]. The textile industries release 10-15% of unfixed dyes which are of higher concentration in effluents [7]. Further, the contact of humans with pesticides can be detrimental causing some serious health issues [8]. Therefore, in order to protect the environment, waste water treatment is of vital importance [9].

1.1 INDUSTRIAL DYE IN WASTE WATER

Dye is a coloured substance that, when connected to a substrate give colour by a process that modifies, any crystal structure of the coloured substances. In almost all the consumer goods sector synthetic dye is prominently used [10]. Yearly, organic dye of ~ 45000 tons is produced worldwide, more than 11% of which is discarded as effluents in water resources [11]. A number of processes ongoing in textile industry like preparation of textile material, dyeing and finishing, are polluting and exploiting natural resources [12]. These waste water create considerable environmental hazards due to their strong colors, greater chemical oxygen demand (80% is because of supplementary dyeing agents like starch and $C_2H_3NaO_2$ and 20% is due to dyes) and the effluents complex chemical nature [13]. Photosynthesis is also being affected as they change the absorption and reflection of sunlight on the water.

1.1.1 METHYLENE BLUE (MB)

Methylene Blue (MB), one of the most commonly used dyes for industrial purposes, such as paint, paper, printing and dyeing, leathers etc. Methylene blue which is also known as methylthioninium chloride, having molecular formula $C_{16}H_{18}ClN_3S$. It is used as dye and medication. Medically, it is used to treat methemoglobinemia. Earlier it was also used to treat Urinary tract infection (UTI) and Cyanide poisoning. As a dye, it is a thiazine dye and because it is a cationic dye, therefore, its adsorption is favoured on a negatively charged surface at high pHs [14]. The λ_{max} of MB Dye comes near 664nm.

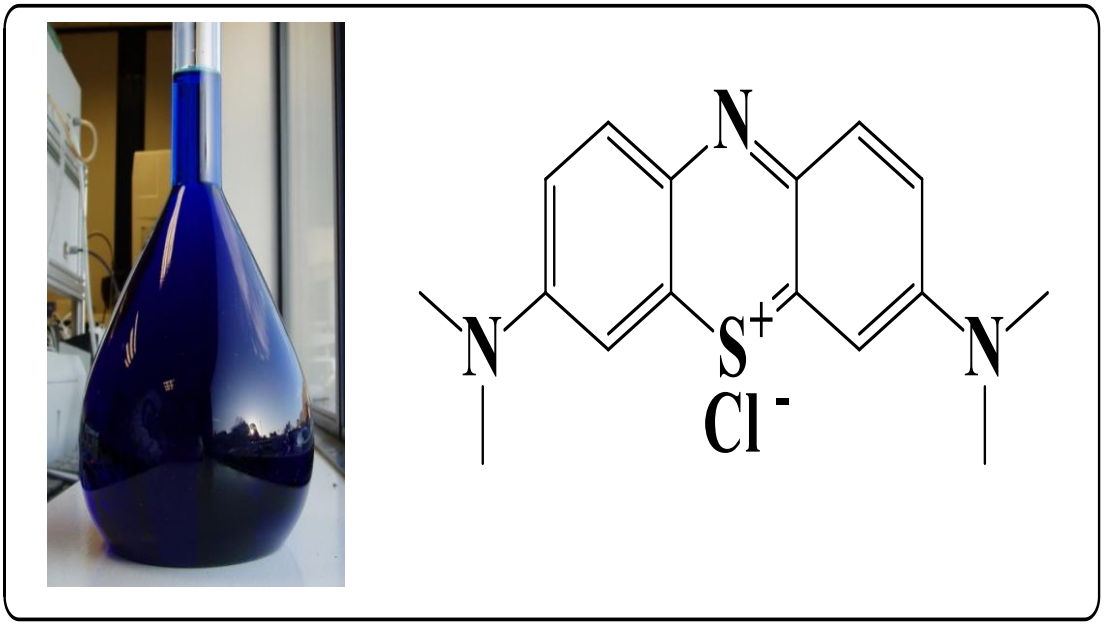

Fig. 1. Structure of Methylene Blue dye

These dyes are not affected by the microbial attack and are also very stable in the presence of sunlight. Thus, these dyes are not degraded easily which is why conventional wastewater treatment systems prove to be less useful to pull them out of water bodies [15].

1.2 TRADITIONAL WASTE WATER TREATMENT

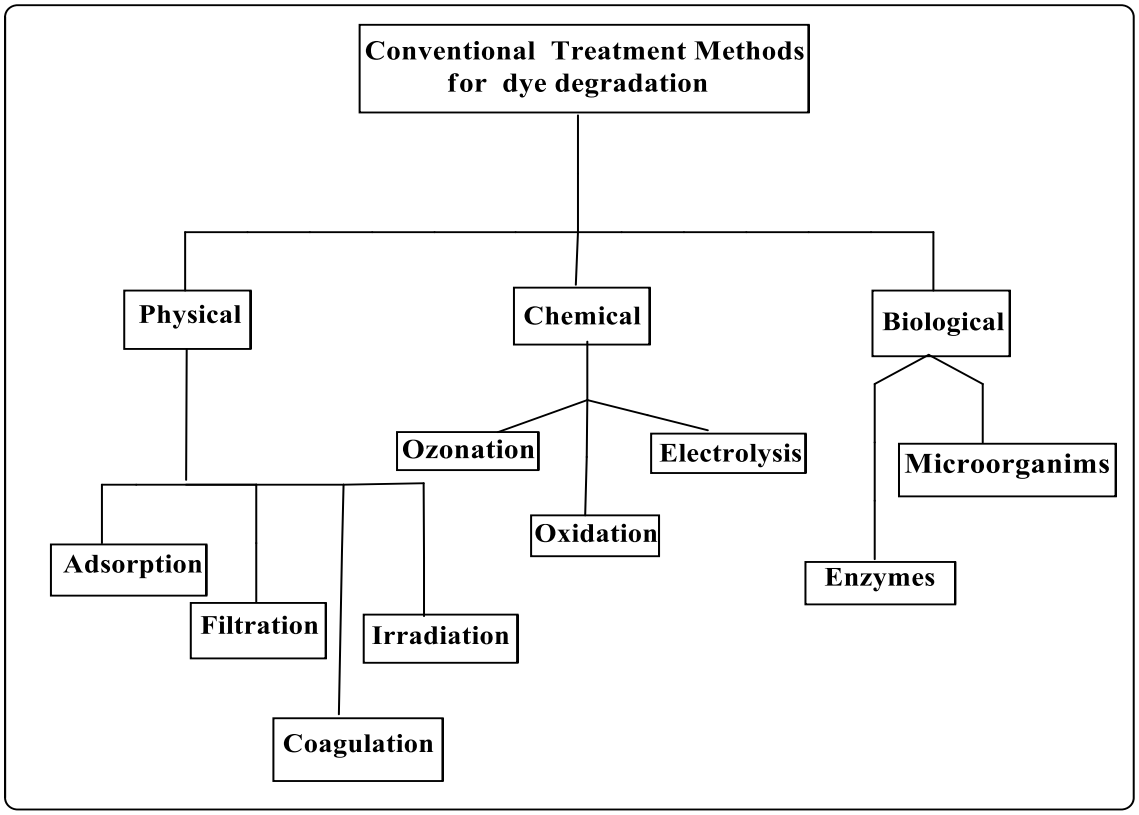

Fig. 2. Outline of Conventional treatment methods used for dye degradation

1. Physical Methods: Physical Methods are employed to separate both heavy materials as well as easily separable materials from wastewater systems [12]. These methods include: (a) Adsorption (b) Filtration (c) Coagulation (d) Irradiation

2. Chemical Methods: Chemical methods can be broadly defined as the methods that use chlorine or chlorine containing substances to carry out the oxidation and disinfection of water reserves. Various chemical methods are given below:

(a) Ozonation

(b) Chemical oxidation

(c) Electrochemical oxidation

(d) Electrolysis

(e)Advanced Oxidation Processes (Photochemical and Photocatalytic)

3. Biological Methods-Biodegradation

Biodegradation is defined as the decomposition of organic compound either aerobically or anaerobically by bacteria, fungi and other microorganisms. It is also called as bio-remediation as for the removal of organic pollutants, microbes are used.

1.2.1 ADVANCED OXIDATION PROCESSES

Advances oxidation processes (AOP) [12] or heterogeneous photocatalysis decomposes the organic pollutants into H_2O and CO_2. This method has proven to be greatly effective as almost complete degradation [16] takes place with a mere requirement of solar or near UV-light [17]. Moreover, this methodology is effective at room temperature [18] with pollutants being completely mineralized [19]. AOP is classified into various categories.

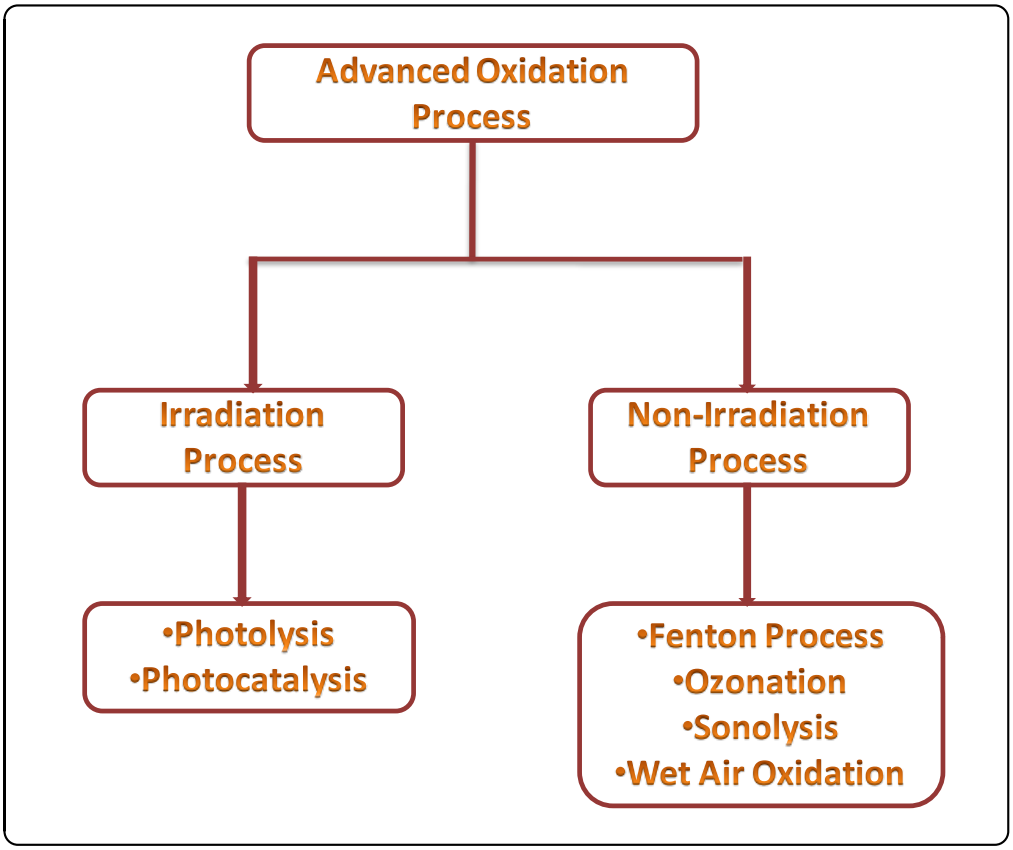

Fig. 3. Classification of Advanced oxidation process

1.3 PHOTOCATALYSIS

Catalyst is a substance which helps to speed up the chemical reaction without being used itself, thus photocatalyst is characterized as a material which accelerates the chemical rate of reaction in the presence of light by forming electron-hole pair which empowers the participants of chemical reaction to transform and recover its chemical composition. "Photocatalysis" can be characterized as the process where the rate of a chemical reaction in light increases by the use of a catalyst.

1.3.1 g-C_3N_4@BiOCL HYBRID (EFFICIENT PHOTOCATALYST)

Amid the various semiconductors, g-C_3N_4 has come across as an outstanding metal-free inorganic semiconductor owing to its non-toxicity, high chemical stability, cost-effectiveness, low band gap (~ 2.7 eV), reducibility and sustainability. These attributes make it a suitable choice as a catalyst for not only photocatalytic degradation but also for water splitting and in biotechnology [20]. However, high recombination rate of g-C_3N_4 restricts an effective photodegradation [21].

BiOCl is a promising non-toxic catalyst having an indirect transmission band gap, stabilized the chemical property, corrosion resistance and open crystalline structure [22]. BiOCl is having open layered structure which consists of $[Bi_2O_2]^{2+}$ layers in between two slabs of halogen ions which provides more space to polarize the related atoms and orbitals and then increases the separation efficiency of photo induced electron-hole pair [22]. But a wide band gap of BiOCl (~ 3.2-3.6 eV) limits its use as it can only be excited in UV radiation [23].

To improve its photocatalytic performance, doping of BiOCl with g-C_3N_4 nanosheets is a great option as an efficient hybrid catalyst is formed. This occurs because of the suitably-matched energy levels of g-C_3N_4 and BiOCl that can overlap in the band structure and it is suitable for the assembly of heterojunction catalyst with visible light response [23].

CHAPTER 2 : LITERATURE REVIEW

The attention has shifted in recent years towards the synthesis of g-C_3N_4@BiOCl hybrid to enhance the photocatalytic activity and the degradation of dye. Thus different types of nanocomposite with g-C3N4 are prepared to degrade the dye. Amid Various photocatalyst, g-C_3N_4@BiOCl which shows high efficiency for degradation of dyes. There are numerous methods to prepare and to optimize g-C_3N_4@BiOCl. In this chapter, an overview of the literature available about g-C_3N_4@BiOCl has been discussed.

Cai, 2015 obtained g- C_3N_4 using urea by heating it directly at 550^oC for 3 h at 10$^oCmin^{-1}$.The composite was synthesized by taking calculated quantity of g-C_3N_4 and is dissolved in 100 mL water and 30 min sonication was done. Bismuth nitrate (2 mmol) was dispersed in 200 mL water, little quantityt of nitric acid was mixed with this solution. This was added dropwise to above solution of g-C_3N_4. The stirring and heating of mixture in water bath for 30 min at 80 ^oC. KCl(2 mmol) was added while constantly for 30 min. The mixture is transferred into hydrothermal vessel and kept for 8 h at 150 ^oC. The product obtained was centrifuged and washed with water and ethanol and dried at 60 ^oC. Thus can be used for degradation of phenol with degradation efficacy of 94% within 150 min with rate constant of 0.0195 min^{-1}[23].

Wang *et al.,* 2018 prepared 2D/2D BiOCl-g-C_3N_4 by a solvothermal method and various techniques were employed for characterization of catalyst like XRD, BET, DRS, FTIR, TEM. The photodegradation of 4-Chlorophenol under visible ligh was done to examine the photocatalytic activity of BiOCl-g-C_3N_4 composite. 50BiOCl-50C_3N_4 show maximum photocatalytic activity with 95% degradation efficiency in 120 min and having a rate constant of 0.0250 min^{-1} [24].

Chang *et al.,* 2014 prepared the composite by facile chemical deposition-precipitation method by taking a mesured amount of g- C_3N_4 with bismuth nitrate into a mixture of HCl, H_2O and propanol and for obtaining the uniform suspension the mixture was sonicated for 0.5 h. NaOH was added dropwise to the solution. After striring and aging for 0.5 h and 6 h, respectively , the resulted precipates were gathered through centrifugation and finally washing with water and ethanol was done, dried out at 100^oC overnight. Thus can be used for degradation of Rhodamine-B dye with rate constant of 0.1170 min^{-1} which is shown by g-C_3N_4@BiOCl-3% [25].

Kang *et al.,* 2016 prepared BiOCl/Au through a chemical process comprising of two-steps at low temperature. The authors degradaded Rhodamine B dye in visible light for 200 min. They observed rate constant of 0.00869 min^{-1}. The increase in performance was because of transfer of electrons from BiOCl to Au as a heterojunction is formed at the interface [26].

Li *et al.,* 2015 formed g-C_3N_4/BiOCl composite by incorporating g-C_3N_4 nanoparticles on BiOCl having unlike (BOC-001 and BOC-010) exposed facets. ng-CN/BOC-010 composite showed improvement in photocatalytic degradation due to proficient separation and migration of photogenerated electron–hole pair. Methyl Orange was Photodegraded to examine the activity of g-C_3N_4/BiOCl in visible light. ng-CN/BOC-010 show degradation efficiency of 10.9% in 150 min having rate constant 0.01838 min^{-1} suggesting this facet orientation is a major factor involving high photocatalytic performance [27].

Xu *et al.,* 2017 synthesised porous g-C_3N_4 by a method without where no additional reagents were used. The rate of degradation of methylene blue was ~6.4 times faster in case of porous g-C_3N_4 (0.009 min^{-1}) than bulk in visible light illumination. Porous g-C_3N_4 has an increased number of active sites, better charge separation and an enhanced efficacy of charge transfer [5].

Cui *et al.,* 2015 synthesised BiOCl nanostructures by employing a non-aqueous solvothermal method making use of ethylene glycol (EG). Hydroxyl radicals generation ability was tested by PL spectroscopy where coumarin was used as fluorescence proble molecule. Methyl orange degradation was conducted to evaluste the photocatalytic performance. The photodegradation rate was higher for BOC-110 and rate constant was 0.0091 min^{-1} in UV light and 0.0070 min^{-1} in visible light. Exposed (110) facets was responsible for high photodegradation efficiency [28].

Dong and Zhang, 2011 prepared g-C_3N_4 by direct heating of melamine and substituting it with melamine hydrochloride leads to porousification in the final g-C_3N_4 which exhibits enhanced surface area and photocatalytic activity. Rhodamine-B was degraded in visible light for 30 min and rate constant is 0.014 min^{-1}[29].

Wang *et al.,* 2013 fabricated BiOCl-C_3N_4 heterojunction via an in situ ionic-liquid-assisted solvothermal method due to which highly dispersed heterojunction was formed. The best photocatalytic activity was shown by 1BiOCl:1C_3N_4 for the photodegradation of Methyl Orange (95% degradation in 80 min) which has 3.3 times better activity than the samples obtained by mechanical mixing [30].

Table 1. Different g-C_3N_4 and BiOCl based catalysts reported in literature.

Photocatalyst	**Catalyst Concentration (g/L)**	**Pollutant degraded (Concentration)**	**Light source**	**Time (min)**	**Degradation efficiency**	**Rate constant (min^{-1})**	**Reference**
50% C_3N_4/BiOCl	1	Phenol (10 ppm)	Visible	150	94%	0.0195	[23]
50% C_3N_4/BiOCl	0.5	4-Chlorophenol (10 ppm)	Visible	120	95%	0.0250	[24]
Au/BiOCl	0.4	Rhodamine-B (4 ppm)	Visible	200	-	0.00869	[26]
g-C_3N_4/BiOCl	0.6	Methyl Orange (20 ppm)	Visible	150	10.9%	0.01838	[27]
g- C_3N_4	1	Rhodamine-B (5 ppm)	Visible	30	-	0.014	[29]
1BiOCl:1C_3N_4	1	Methyl Orange (10 ppm)	Visible	80	95%	-	[30]

CHAPTER 3: MATERIALS AND METHODOLOGY

3.1 MATERIALS AND REAGENTS

Bismuth nitrate and potassium chloride were purchased from Loba Chemie Pvt Ltd. Melamine and Imidacloprid were obtained from Sigma-Aldrich. Methylene blue was acquired from Merk. The chemicals used were of analytical grade and were used without further purification. The water was used was deionized for the preparation of solutions during the experiments.

3.2 PREPARATION OF g-C_3N_4 NANOSHEETS

Firstly, bulk g-C_3N_4 was prepared by heating melamine in a muffle furnace with a heating rate of 2.5 ºC min^{-1} for 4 h at 550 ºC. About 0.5 g of bulk g-C_3N_4 was ultrasonically dispersed in 40 mL of water for 1 h and stirred for 3-4 h. The dispersed solution was poured in Teflon line autoclave with a heating rate of 5 ºC min^{-1} for 12 h at 180 ºC in an oven. The suspension was centrifuged and washed with deionized water for 4-5 times and dried at 60 ºC overnight. The obtained porous g-C_3N_4 was pale yellow in colour, it was kept in a crucible and heated in a muffle furnace with a heating rate of 5 ºC min^{-1} for 2 hrs at 500 ºC. The obtained white powder was g-C_3N_4 Nanosheets (NS) [5].

3.3 SYNTHESIS OF g-C_3N_4@BiOCL COMPOSITE

Measured amount of g-C_3N_4 NS (92, 92, 276 mg for 1:1, 1:3 & 3:1, respectively) was dissolved in 100 ml water by ultrasonication for 30 min. Calculated amount of bismuth nitrate (485, 1455.2, 485 mg for 1:1, 1:3 & 3:1, respectively) was dissolved in 200 mL water, subsequently, and a small amount of nitric acid was added to it. This solution was dropwise added to the above g-C_3N_4 suspension. The obtained blend was stirred and sonicated for 1 h and later measured amount of KCl (74.5, 223.6, 74.5 mg for 1:1, 1:3 & 3:1, respectively) was added to it and the final mixture was stirred overnight. Then, it was centrifuged and washed with water and ethanol several times and dried in a hot air oven at 60 ºC. In this way different ratios g-C_3N_4@BiOCl hybrid is formed. Scheme 1 illustrates pictorially the preparation of bulk g-C_3N_4, porous g-C_3N_4, g-C_3N_4 nanosheets, and g-C_3N_4@BiOCl hybrid.

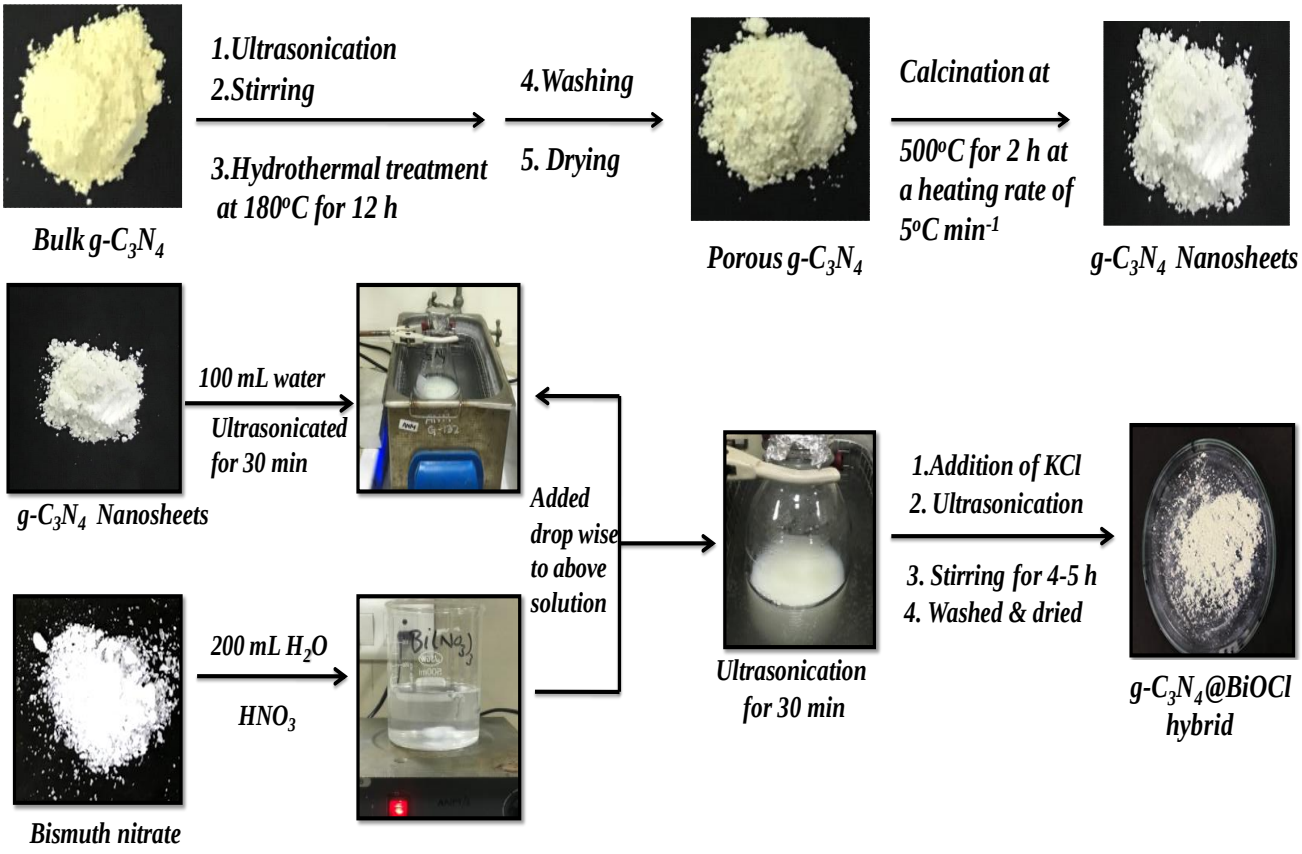

Scheme 1. Synthetic scheme for the preparation of bulk, porous, nanosheets of g-C_3N_4 and g-C_3N_4@BiOCl hybrid.

3.4 CATALYST CHARACTERIZATION

The X-Ray Diffraction analysis (XRD) of g-C_3N_4@BiOCl catalyst was done by means of PANalytical X-ray diffractometer with Ni-filtered Cu Kα radiations (λ = 0.1504 nm) with a scan rate of 2° min^{-1} and range of 10–90° at 45 kV. The BET surface area analyzer from Microtrac Belsorp Mini-II (Bel, Japan, Inc) was employed for the estimation of the surface area of the compounds, at -196 °C. To get rid of trapped impurities, the samples were first pre-treated at 100 °C for 5-6 h. Barrett–Joyner–Halenda (BJH) method was used to know the pore size distribution from N_2 adsorption-desorption isotherms. The photocatalytic performance was monitored using a UV spectrophotometer (Champion) from 200 to 800nm and UV–Vis DRS was performed using diffuse absorbance mode through Hitachi-3900H spectrophotometer. Photoluminescence (PL) spectroscopic studies were carried out using Perkin Elmer LS-55, USA (excitation wavelength = 375 nm). The thermogravimetric analysis (TGA) of the as-synthesized materials was done with a

TA Q500, USA thermal analyzer under continuous N_2 flow (50 mL min^{-1}). FESEM has been used for studying the surface morphology of the as-prepared hybrid through using a ZEISS at an accelerating voltage of 5 kV. XPS spectrometer (Omicron ESCA +) was used to determine the chemical bonding state of the hybrid, through Al Kα radiation (hν = 1487.6 eV).

3.5 PHOTOCATALYTIC STUDY

The as-synthesized photocatalysts were scrutinized under sunlight for their photocatalytic performance. In a typical experiment, 2mg of catalysts were mixed with 10 mL of 5 ppm MB. For achieving the adsorption-desorption equilibrium, the suspension was stirred for 30 min in dark and later irradiated with bright sunlight for 70 min. The experiments were conducted during the first 15 days of April, 2019 during the daytime under bright sunlight exposure at TIET, Patiala, India. The average solar radiation of ~ 600 W/m^2 was measured by Pyranometer (LICOR), USA. The samples were analyzed by using UV-Vis spectrophotometer at regular intervals after the separation of catalyst from the solution to monitor the absorbance band of MB at λ_{max} = 664. The following equation was used to calculate the degradation efficiency:

Degradation efficiency or % Degradation = $\{(A_0 - A) / A_0\} \times 100$

4.1 XRD ANALYSIS

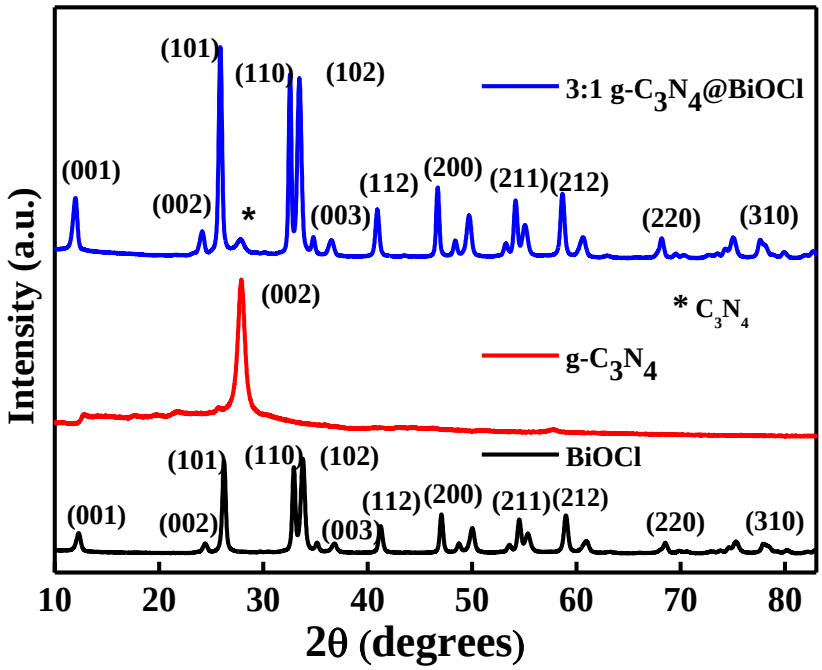

Fig. 4. XRD spectra of BiOCl, g-C_3N_4 and 3:1 g-C_3N_4@BiOCl

The XRD patterns of pure g-C_3N_4, BiOCl and g-C_3N_4@BiOCl are presented in Fig. 4. Pure g-C_3N_4 exhibits a strong peak at 27.6º due to (002) plane corresponds to characteristic interlayer-stacking peak of the aromatic system [31]. The characteristics diffraction peaks of BiOCl are observed at 2θ ~ 12.32º, 24.40º, 26.09º, 32.70º, 33.79º, 36.61º, 41.11º, 46.94º, 49.93º, 54.56º, 58.93º, 68.45º, 75.06º, 77.56º corresponding to (001), (002), (101), (110), (102), (003), (112), (200), (113), (211), (212), (220), (214) and (310) and one additional peak at 27.81º is observed in case of hybrid g-C_3N_4@BiOCl which corresponds to (002) plane. Absence of any impurity peak indicates the high purity of synthesized hybrid without the formation of any side product.

4.2 XPS ANALYSIS

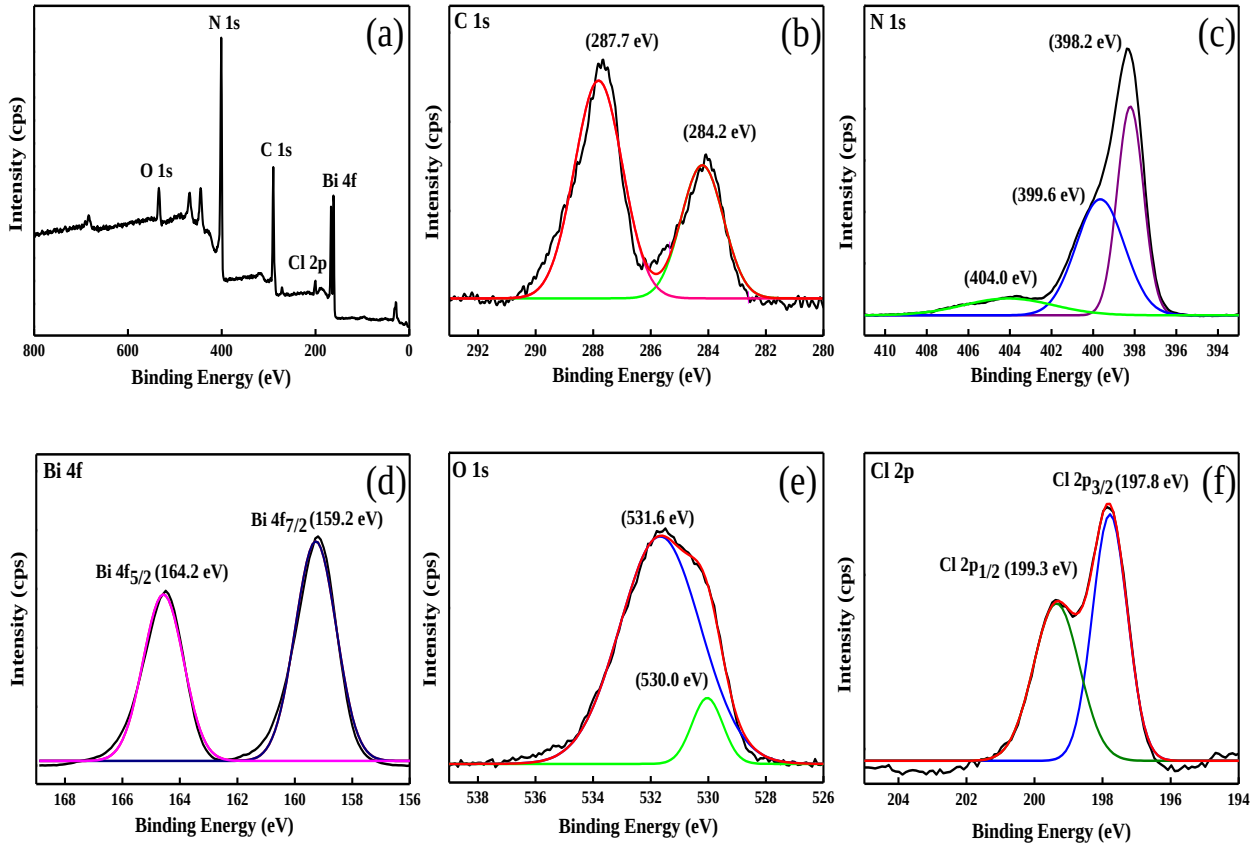

Fig. 5. (a-f) XPS spectra of C_3N_4@BiOCl composite; (a) a typical survey spectra, deconvoluted peaks for (b) C 1s, (c) N 1s, (d) Bi 4f, (e) O 1s and (f) Cl 2p.

To know the chemical states and surface chemical composition of g-C_3N_4@BiOCl, XPS measurements were performed. The high-resolution spectra of C 1s, N 1s, Bi 4f, O 1s, Cl 2p were shown in Fig. 5. The C 1s spectra show two peaks at 287.7 eV and 284.2 eV corresponding to N=C-N of triazine rings and graphitic carbon on g-C_3N_4 surface respectively [23]. XPS of N 1s exhibits three peaks; the peak at binding energy of 398.2 eV is due to sp^2 hybridized N involved in triazine ring [25], the peak at 399.6 eV could be due to C-(NH) and the peak at 404 eV is due to C $\equiv$N [23]. For Bi, the peaks at 159.2 and 164.5 eV which correspond to the Bi $4f_{7/2}$ and Bi $4f_{5/2}$ and are characteristic of Bi^{3+} in BiOCl material [25]. In the given figure O 1s peak is obtained at 530 and 531.6 eV and Cl 2p are at 197.8 eV (Cl $2p_{3/2}$) and 199.3 eV (Cl $2p_{1/2}$).

4.3 N_2 ADSORPTION-DESORPTION STUDIES

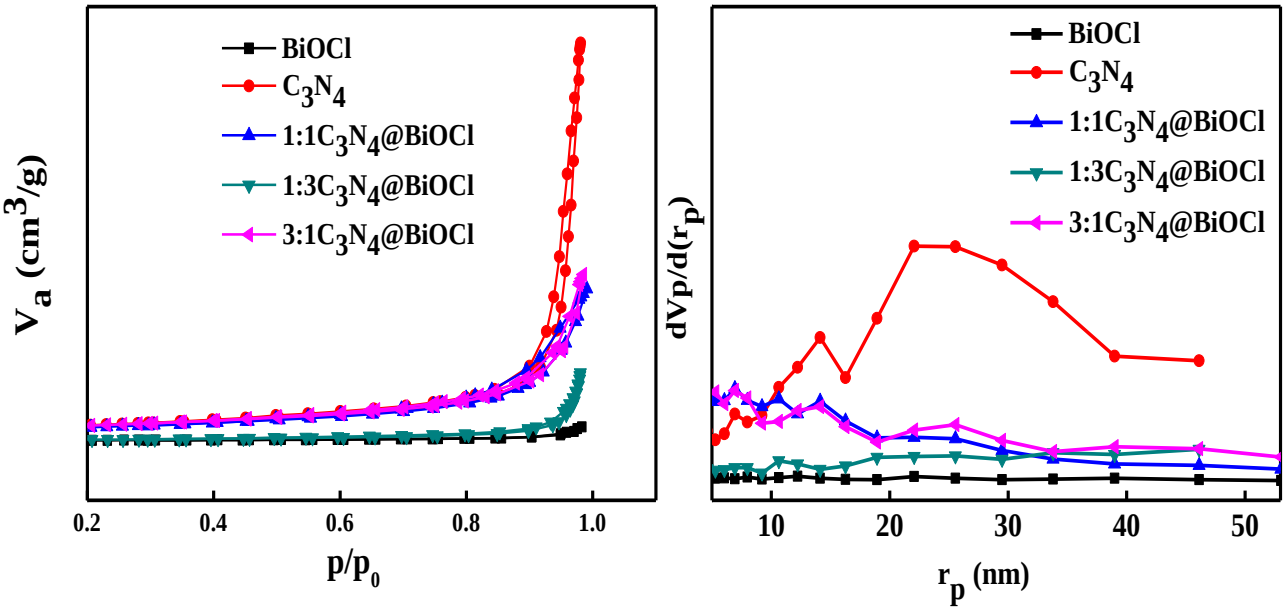

Fig. 6. (a) N_2 adsorption-desorption isotherm, (b) BJH

Surface properties of the as-synthesized catalysts were analyzed by BET analysis. All the samples showed a Langmuir type-IV isotherm which signified their mesoporous nature as shown in Fig 6(a). The BJH plot describes the pore size distribution (Fig 6b). The sharp peaks in the mesoporous range clearly indicate the existence of mesopores in the as-prepared catalysts. The surface area, total pore volume and mean pore diameter of the synthesized catalysts have been enlisted in Table 1. The 3:1 g-C_3N_4@BiOCl had the highest surface area (~107 m^2/g) among all.

Table 2. Surface properties of the as-synthesized catalysts.

Sample	Surface Area (m^2/g)	Total Pore Volume (cm^3/g)	Mean pore diameter (nm)
BiOCl	11	0.098	14.68
C_3N_4 NS	102	1.063	41.67
1:1C_3N_4@BiOCl	92	0.406	17.70
1:3C_3N_4@BiOCl	17	0.184	44.12
3:1C_3N_4@BiOCl	107	0.987	17.7

4.4 THERMOGRAVIMETRIC ANALYSIS (TGA)

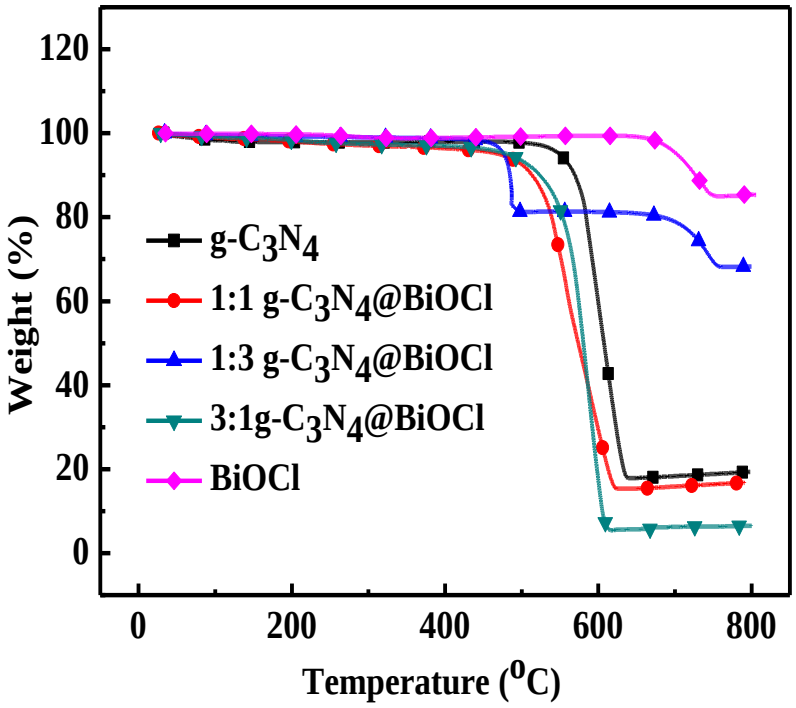

Fig. 7. TGA plot of g-C_3N_4, BiOCl and various composites

Thermogravimetric analysis was carried out in N_2 atmosphere (50 mL min^{-1}). The samples were heated from room temperature to 800°C at 5°C min^{-1}. As shown in Fig. 7, the first weight loss (~14%) for pure BiOCl occurs at 640 °C. In the case of g-C_3N_4 nanosheets, first weight loss ~ 2% occurs at 50-100°C possibly due to water loss and the second decomposition occurs at 540°C having a weight loss of ~80%. The composite 1:1 g-C_3N_4@BiOCl exhibits first decomposition at 50°C due to dehydration of water and second weight loss (~78%) at 500 °C. In the case of 1:3 g-C_3N_4@BiOCl, decomposition starts at 450 °C with ~18% weight loss and followed by decomposition at 678 °C with ~12% weight loss. First decomposition in 3:1 g-C_3N_4@BiOCl occurs at 50 °C due to water loss and second at 490 °C with a weight loss of 89%.

4.5 FESEM AND HRTEM

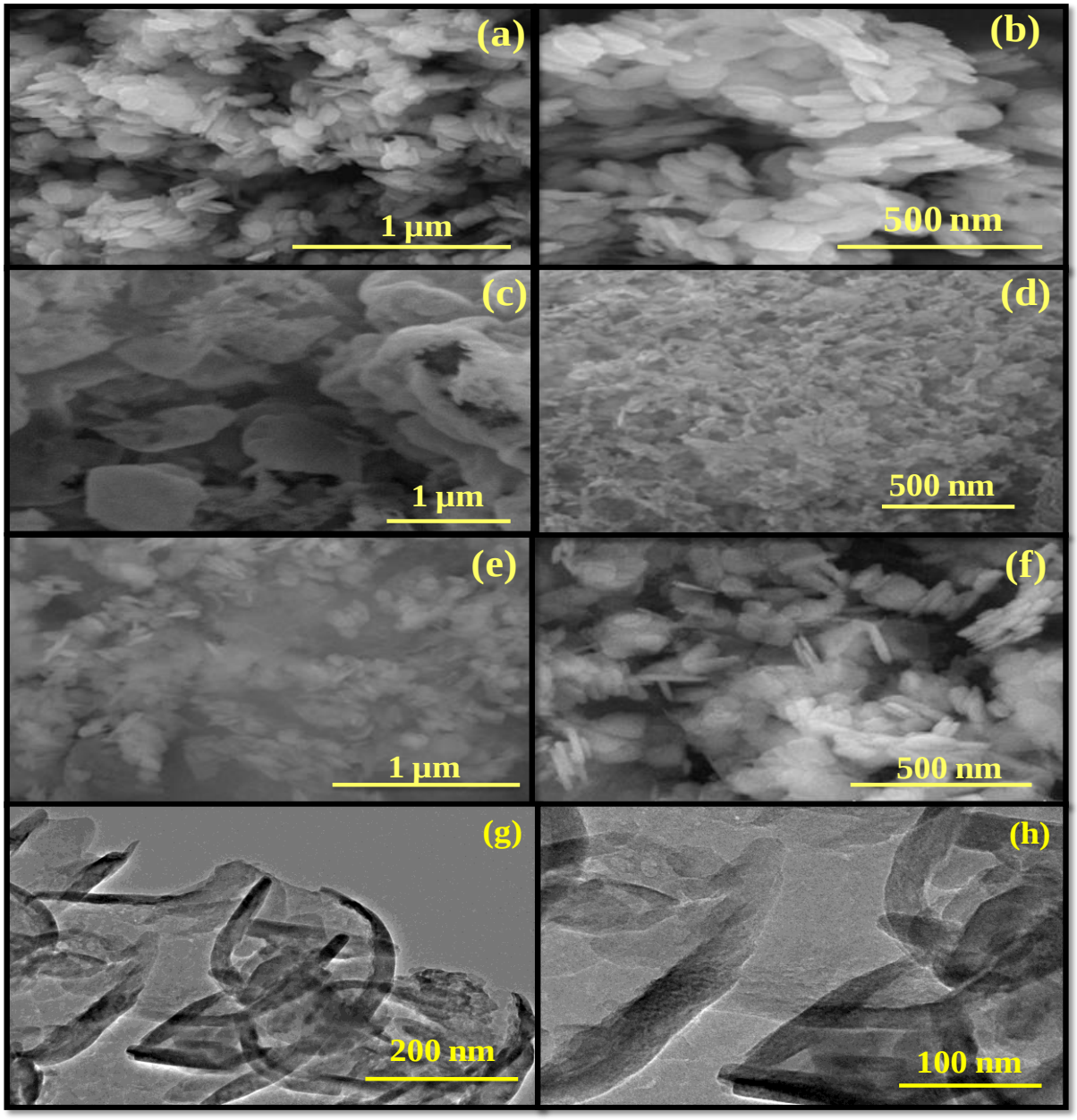

Fig. 8. FESEM images of (a-b) BiOCl; (c-d) g-C_3N_4 nanosheets, and (e-f) g-C_3N_4 @BiOCl composite (g-h) HRTEM images of g-C_3N_4@BiOCl hybrid at different magnification.

The surface morphology of as-synthesized materials was analyzed by FESEM images as displayed in Fig.8 (a-h). It is evident from Fig. 8(a-b) that BiOCl platelets were formed and had a smooth surface. The g-C_3N_4 nanosheets are noticeable in Fig. 8(c-d) which helps in increasing the surface area. Fig. 8(e-f) depicts the FESEM image of 3:1 g-C_3N_4@BiOCl hybrid. It can be seen that the

surface of BiOCl platelets is well-covered with g-C_3N_4 nanosheets. Moreover, the HRTEM images (Fig. 8g, h) confirm the platelets like morphology of BiOCl and sheets like g-C_3N_4.

4.6 EDX AND ELEMENTAL MAPPING

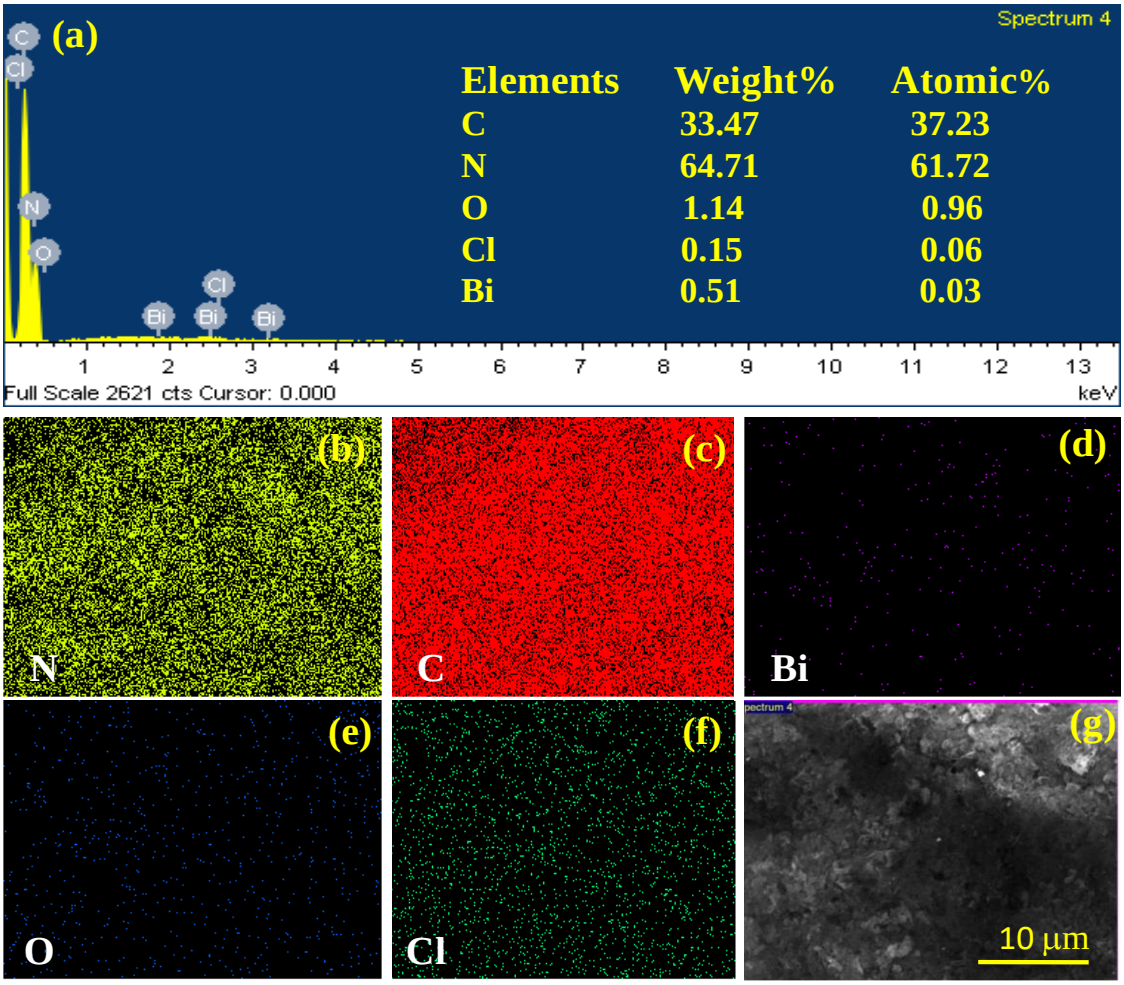

Fig. 9. (a) EDX spectra; elemental color mapping of (b) N; (c) C; (d) Bi; (e) O; (f) Cl, and (g) SEM micrograph.

EDX analysis and elemental mapping of g-C_3N_4@BiOCl is displayed in Fig. 9(a). It validates that C, N, Bi, O, Cl respectively are present in synthesized composite. The elemental color mapping of the hybrid (Fig. 9(b-f)) shows homogeneous distribution of all the elements (C, N, Bi, O, Cl) present in the hybrid. Fig. 9(g) shows the SEM micrograph of the g-C_3N_4@BiOCl hybrid.

4.7 PHOTOLUMINESCENCE & UV-VISIBLE DRS SPECTROSCOPY

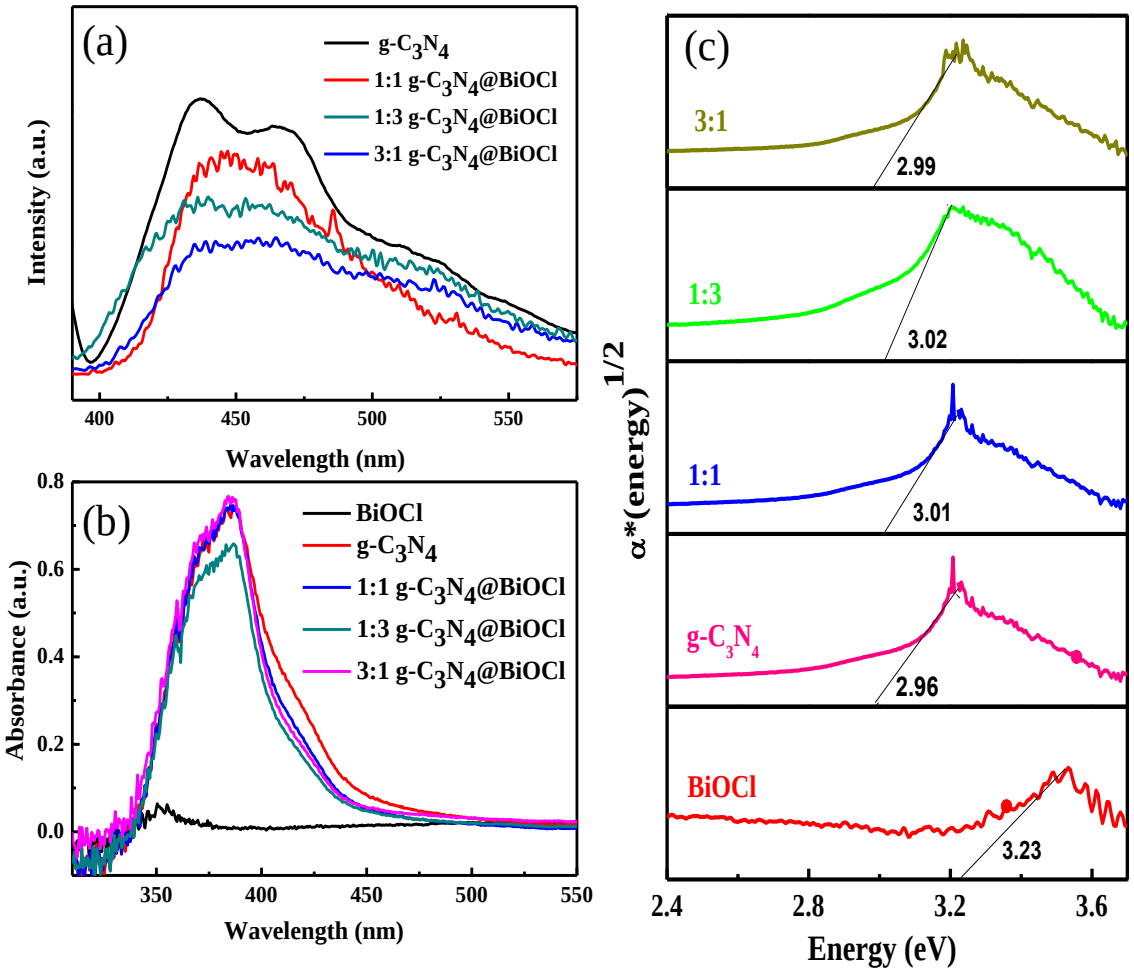

Fig. 10. (a) Photoluminescence spectra (b) UV-Visible diffuse reflectance spectra, and (c) Tauc plot of the as-synthesized catalysts.

The low recombination rate of electron-hole in a photoactive semiconductor has a chief role in the photocatalytic performance. PL analysis was used to scrutinize the migration of charge carriers in semiconductors [32]. The excitation peak used for PL analysis of the materials was 375 nm (Fig. 10a). The emission peak of g-C_3N_4 comes out at around 456 nm in visible light range and is good in accordance with a band gap of g-C_3N_4. Pure g-C_3N_4 shows the highest intensity among various catalysts. The minimum intensity peak is of 3:1 g-C_3N_4@BiOCl which implies that the recombination rate is greatly suppressed in this hybrid and proficient separation of charge carriers is achieved.

The optical absorbance properties of the as-synthesized materials were evaluated by using UV−Vis diffuse reflectance spectroscopy (DRS). The band gap absorption edge of g-C_3N_4 occurs at 456 nm and BiOCl at 365 nm (Fig. 10b). The corresponding band gap energies were determined by using Tauc's relation:

$$(\alpha h\nu)^{1/2} = A(h\nu - E_g)$$

Where α, hν, A and E_g are the absorption coefficient, photon energy, constant and optical band gap, respectively [25]. The band gap energies of g-C_3N_4 and BiOCl from the Tauc plot (Fig. 10c) were estimated to be 2.96 eV and 3.23 eV, respectively. Among various hybrids formed, the band gap of best comes out to be 2.99 which correspond to 3:1 g-C_3N_4@BiOCl.

4.8 PHOTOCATALYTIC DEGRADATION OF MB

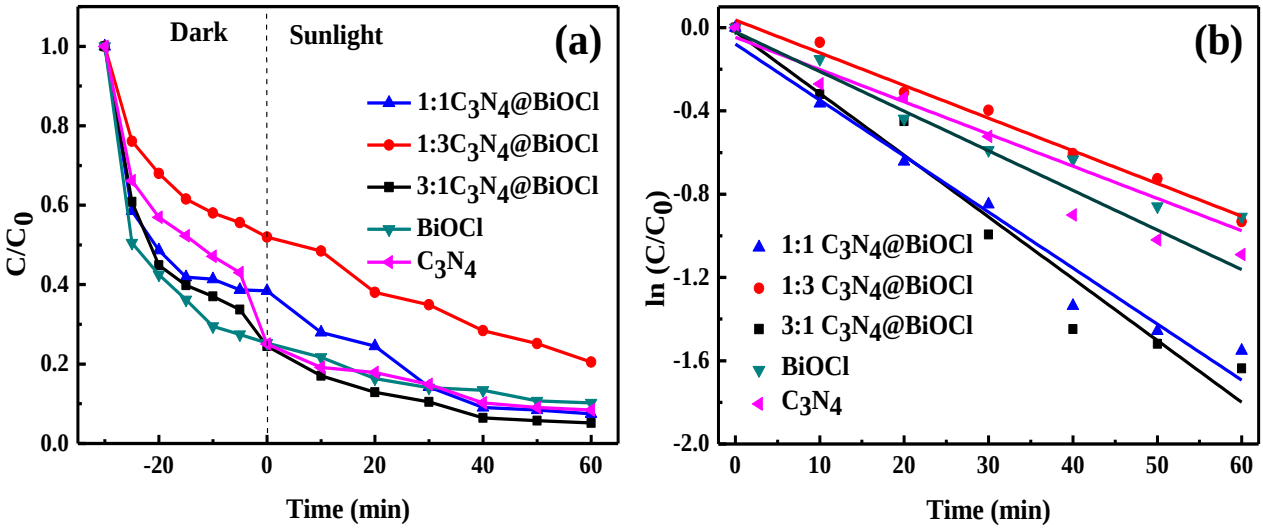

Fig. 11. (a-b) Kinetic analysis for the photodegradation of MB

The photocatalytic activity was scrutinized through the degradation of MB and Imidacloprid under sunlight irradiation. In a typical experiment, 2 mg of catalyst was mixed with 10 mL of 5 ppm MB. The stirring of the solution in dark for 30 min assured the establishment of adsorption-desorption equilibrium and then the dye solution was illuminated with bright sunlight for 70 min. The experimental data were fitted by pseudo-first order reaction model to investigate the reaction

kinetics of MB degradation and the rate constant was evaluated using the following equation: $\ln (C/C_0) = -kt$

Where k is the rate constant, C_0 and C are the concentrations of MB in solution at times 0 and t respectively. Fig. 6(a-b) shows the kinetic analysis of the photodegradation of MB. The degradation efficiency and rate constant of the as-prepared catalysts follows the order: 3:1 > 1:1 > g-C_3N_4 > BiOCl > 1:3 g-C_3N_4@BiOCl. The best catalytic activity out of all the synthesized catalysts was 3:1 g-C_3N_4@BiOCl i.e., 94.8% degradation efficiency and an excellent rate constant of 0.0301 min^{-1}. So, further experiments were carried out using the hybrid 3:1 g-C_3N_4@BiOCl.

4.9 EFFECT OF pH

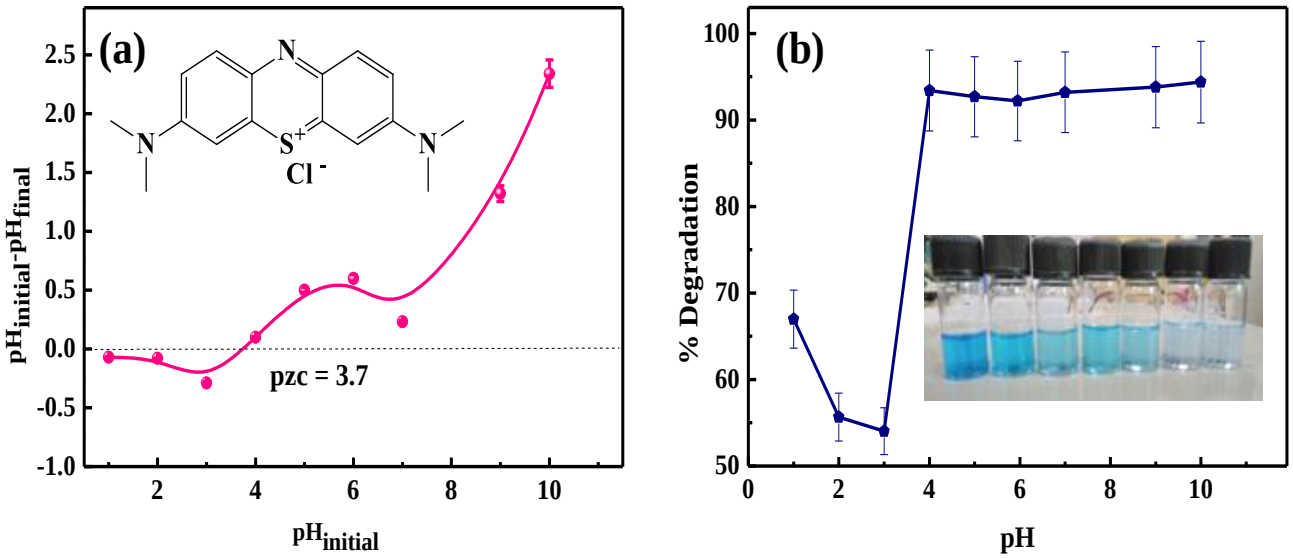

Fig. 12. (a) pzc measurement, (b) effect of pH.

To perceive the effect of pH on the photocatalytic performance, two experiments were conducted: (a) the pzc measurement and (b) photodegradation experiment of MB at different pH using the synthesized photocatalyst. The solution of MB was prepared at different pH (pH 1-10) by addition of 0.1N NaOH and 0.1N HCl accordingly. From the pzc measurement, it was observed that pzc for 3:1 g-C_3N_4@BiOCl was at ~ pH 3.7 (Fig. 12a). This implies that the cationic adsorbents like MB would be adsorbed better above pH 3.7 as the surface of the g-C_3N_4@BiOCl catalyst would become negative above pzc [26]. Fig. 12(b) shows the plot of photodegradation of MB at different pH using 3:1 g-C_3N_4@BiOCl catalyst. The results are in accordance with the pzc value as it can

be seen that the degradation of MB (cationic dye) is very poor below pzc but excellent in neutral and basic pH i.e., above pzc (pH 3.7).

4.10 EFFECT OF CATALYST CONCENTRATION

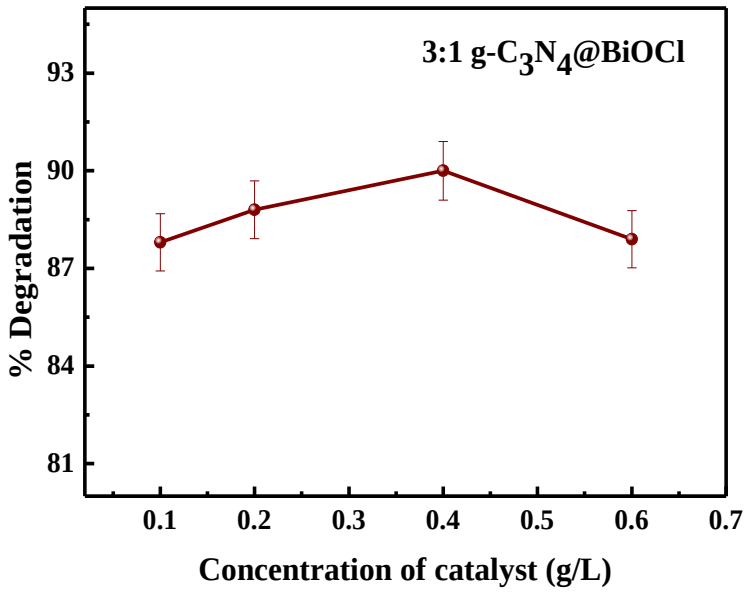

Fig. 13. Plot showing effect of catalyst concentration

To study the effect of concentration of photocatalyst on the photodegradation of MB, various concentrations of 3:1 g-C_3N_4@BiOCl (0.1 g/L to 0. 6 g/L) were taken. The surveillance shows that the degradation efficacy increases when the concentration of catalyst increases from 0.1g/L to 0.4 g/L and thereafter the increase is relatively small (Fig. 13). This is due to the scattering of light and rise in the opacity of the solution.

4.11 REUSABILITY & TRAPPING EXPERIMENT OF PHOTOCATALYST

For the mechanistic studies, various scavengers such as ascorbic acid, methanol, DMSO were employed to trap superoxide radicals ($O_2^{\bullet-}$), holes (h^+) and hydroxyl radicals ($^{\bullet}OH$), respectively to observe the active species in the MB photodegradation process [32]. The degradation efficiency was compared with and without scavenger. It is evident from Fig. 14(a) that the photocatalytic degradation of MB by as-prepared composite was affected only to a small extent by the addition of DMSO and methanol, implying that $^{\bullet}OH$ and h^+ have a minimal role in the process. It was

decreased to the maximum extent in the presence of the ascorbic acid solution which reveals that superoxide radicals play a vital role in dye degradation.

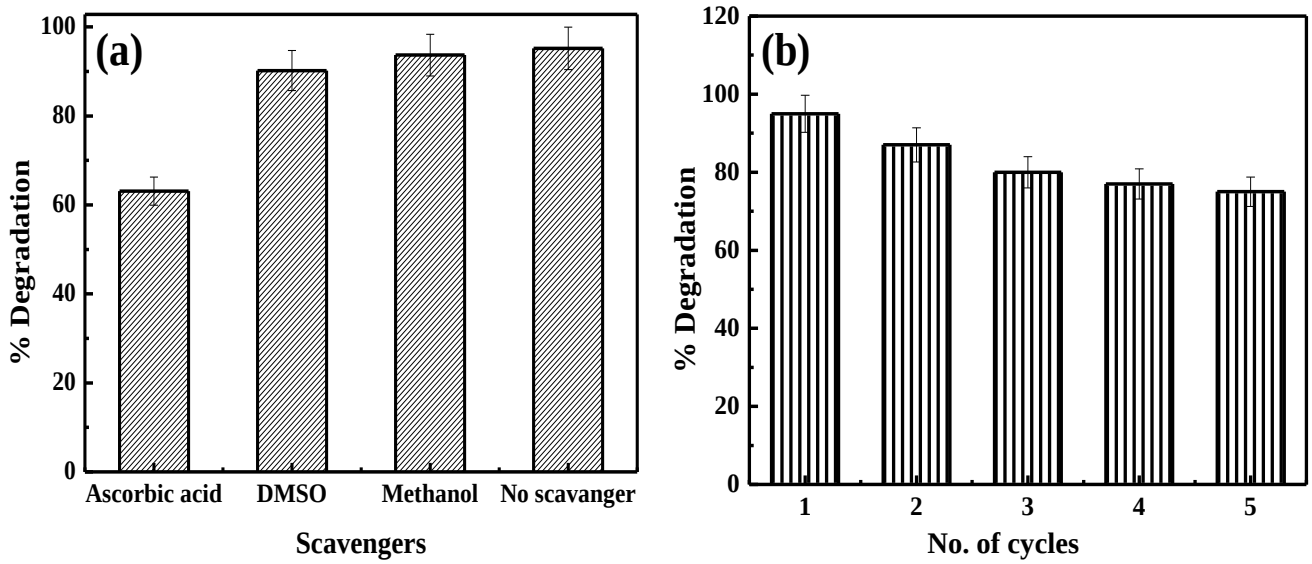

Fig. 14. (a) Effect of scavengers on photodegradation of MB, (b) Reusability studies

From a practical application view, the vital factor is the photocatalyst lifetime. Hence it is needed to measure the photocatalytic stability of the synthesized catalyst for multiple experiment cycles (5 cycles) of degradation. In this context repeated cycle of an experiment for MB removal with g-C_3N_4@BiOCl were carried out to scrutinize its stability. The 3:1 g-C_3N_4@BiOCl catalyst could be separated from the MB suspension effortlessly as the dye got only physically adsorbed on the catalyst surface. After each cycle, the catalyst was separated by centrifugation and washed with water. It can be seen that catalyst has high degradation efficiency (~76%) even after 5 repeated cycles (Fig. 14b).

4.12 PLAUSIBLE MECHANISM FOR MB DEGRADATION

Due to the successful separation of the photogenerated electron-hole pairs, there is augmentation of performance of the g-C_3N_4@BiOCl hybrid. The scheme for sunlight-driven electron-hole separation of the composite is shown in Scheme 2. In sunlight, g-C_3N_4 is easily excited and produce photogenerated electron-hole pairs, whereas BiOCl fails to produce any charges due to the wide band gap (~ 3.23 eV). Photoproduced electrons are prone to move from the conduction band of g-C_3N_4 to that of BiOCl. The CB and VB edge potentials of BiOCl were at 0.23eV and

3.46eV [21] and those of g-C_3N_4 are at -1.26eV and 1.70eV [16] respectively. It is observed that Conduction band edge potential of g-C_3N_4 (-1.26eV) was more negative than of BiOCl (0.23eV), hence the photoinduced electrons on the g-C_3N_4 particle surface get transferred easily to BiOCl [31]. As a result, the electrons could be trapped by the available surface O_2 to initiate the yield of reactive species, such as superoxide anion radical ($O_2^{\bullet-}$) which reacts with water to yield $^{\bullet}OH$ [32]. Both $O_2^{\bullet-}$ and $^{\bullet}OH$ radicals can effectively decompose the pollutants into degraded products. Moreover, the photoinduced holes were suspended in g-C_3N_4 due to the larger difference in VB edge potentials and they can directly get oxidised and decompose the contaminant.

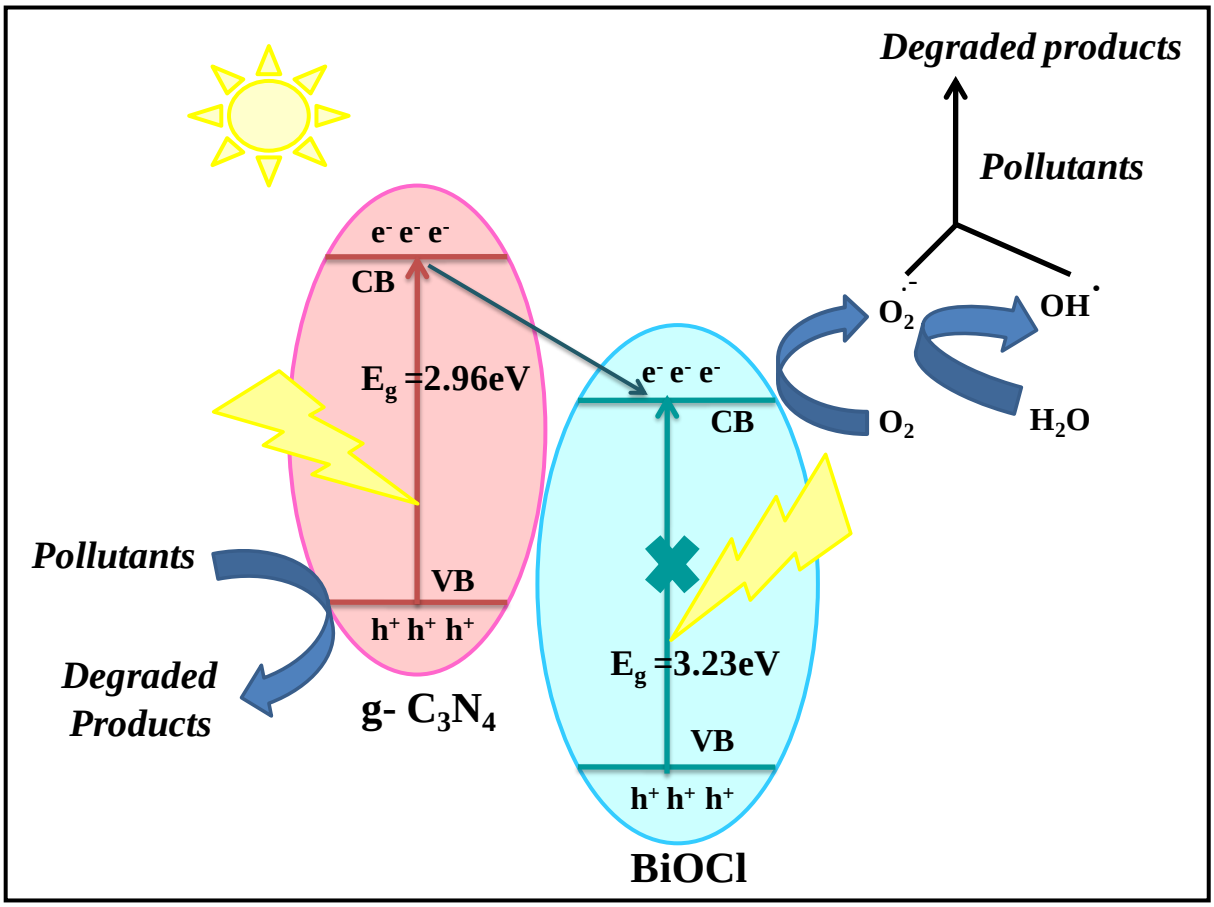

Scheme 2. Plausible mechanism for the photodegradation of MB by g-C_3N_4@BiOCl hybrid.

CHAPTER 5: CONCLUSION

A rapid and simplistic approach was used to synthesize various weight ratios of g-C_3N_4@BiOCl hybrid. The characterization of the hybrid by various techniques revealed the successful formation of the pure material. The hybrid had high surface-area and favouring optical properties i.e., low band gap and recombination-rate. Photocatalytic activity of the as-prepared catalysts was evaluated by the photodegradation of MB in natural sunlight. Out of all the prepared composites, 3:1 g-C_3N_4@BiOCl exhibited the best efficiency. The photocatalyst was also tested for reusability, the effect of pH and catalyst concentration. The possible photocatalytic mechanism was proposed based on trapping experiments revealing that superoxide anion radical plays a pivotal role in the photocatalytic process. This present work shows that g-C_3N_4@BiOCl hybrid is an exceptional photocatalyst as a very small amount of it can degrade noxious pollutants in natural sunlight.

CHAPTER 6: REFERENCES

1. J. Singh, S. Sharma, A. Rathi, S. Basu, Synthesis of Fe_2O_3/TiO_2 monoliths for the enhanced degradation of industrial dye and pesticide via photo-Fenton catalysis, Journal of Photochemistry and Photobiology A: Chemistry, 376 (2019) 32-42.
2. S. Boumaza, B. Bellal, A. Boudjemaa, M. Trari, Photodegradation of orange G by the hetero-junction x%Bi_2S_3 /TiO_2 under solar light, Solar Energy, 139 (2016) 444-451.
3. G. K. Ramesha, A. V. Kumara, H. B. Muralidhara, S. Sampath, Graphene and graphene oxide as effective adsorbents toward anionic and cationic dyes, Journal of Colloid and Interface Science, 361 (2011) 270-277.
4. F. Liang, Y. Zhu, Enhancement of mineralization ability for phenol via synergetic effect ofphotoelectrocatalysis of g-C_3N_4 film, Applied Catalysis B: Environmental, 180 (2016) 324-329.
5. J. Xu, Z. Wang, Y. Zhu, Enhanced visible-light-driven photocatalytic disinfection performance and organic pollutant degradation activity of porous g-C_3N_4 nanosheets, ACS Applied Materials & Interfaces, 9 (2017) 27727-27735.
6. A. Gupta, O. P. Pandey, Visible irradiation induced photodegradation by NbC/C nanocomposite derived from smoked cigarette litter (filters), Solar Energy, 163 (2018) 167-176.
7. M.A. Hassaan, A. El Nemr, Health and Environmental Impacts of Dyes: Mini Review, American Journal of Environmental Science and Engineering, 1 (2017) 64.
8. A. Rathi, S. Basu, S. Barman, Adsorptive removal of fipronil from its aqueous solution by modified zeolite HZSM-5: Equilibrium, kinetic and thermodynamic study, Journal of Molecular Liquids, 283 (2019) 867-878.
9. A. Mishra, A. Mehta, M. Sharma, S. Basu, Enhanced heterogeneous photodegradation of VOC and dye using microwave synthesized TiO_2/Clay nanocomposites: A comparison study of different type of clays, Journal of Alloys and Compounds, 694 (2017) 574-580.
10. J. Šíma, P. Hasal, Photocatalytic degradation of textile dyes in a TiO_2/UV system, Chemical Engineering, 32 (2013) 79-84.
11. E. Forgacs, T. Cserhati, G. Oros, Removal of synthetic dyes from wastewaters: a review, Environment international, 30 (2004) 953-971.

12. Y. Anjaneyulu, N. S. Chary, D. S. S. Raj, Decolourization of industrial effluents–available methods and emerging technologies–a review, Reviews in Environmental Science and Bio/Technology, 4 (2005) 245-273.
13. X. Zhang, Y. Wu, G. Xiao, Z. Tang, M. Wang, F. Liu, X. Zhu, Simultaneous photocatalytic and microbial degradation of dye-containing wastewater by novel g-C_3N_4-P25/photosynthetic bacteria composite, PloS one, 12 (2017) e0172747.
14. H. Lachheb, E. Puzenat, A. Houas, M. Ksibi, E. Elaloui, C. Guillard, J. M. Herrmann, Photocatalytic degradation of various types of dyes (Alizarin S, Crocein Orange G, Methyl Red, Congo Red, Methylene Blue) in water by UV-irradiated titania, Applied Catalysis B: Environmental, 39 (2002) 75-90.
15. W. Z. Tang, H. An, UV/TiO_2 photocatalytic oxidation of commercial dyes in aqueous solutions, Chemosphere, 31 (1995) 4157-4170.
16. M. Petala, V. Tsiridis, P. Samaras, A. Zouboulis, G. P. Sakellaropoulos, Wastewater reclamation by advanced treatment of secondary effluents, Desalination, 195 (2006) 109-118.
17. M. A. Rauf, S. S. Ashraf, Fundamental principles and application of heterogeneous photocatalytic degradation of dyes in solution, Chemical engineering journal, 151 (2009) 10-18.
18. M. R. Hoffmann, S. T. Martin, W. Choi, D. W. Bahnemann, Environmental applications of semiconductor photocatalysis, Chemical reviews, 95 (1995) 69-96.
19. F. Esther, C. Tibor, O. Gyula,Removal of synthetic dyes from wastewaters: a review, Environment international, 30 (2004) 953-971.
20. J. Singh, P. Kumari, S. Basu, Degradation of toxic industrial dyes using SnO_2/g-C_3N_4 nanocomposites: Role of mass ratio on photocatalytic activity, Journal of Photochemistry and Photobiology A: Chemistry, 371(2019) 136-143
21. A. Mishra, A. Mehta, S. Basu, N.P. Shetti, K.R. Reddy, T.M. Aminabhavi, Graphitic carbon nitride (g-C_3N_4)-based metal-free photocatalysts for water splitting: A review, Carbon, 149 (2019) 693-721.
22. Q. Wang, W. Wang, L. Zhong, D. Liu, X. Cao, F. Cui, Oxygen vacancy-rich 2D/2D BiOCl-g-C_3N_4 ultrathin heterostructure nanosheets for enhanced visible-light-driven photocatalytic activity in environmental remediation, Applied Catalysis B: Environmental, 220 (2018) 290-302.
23. L. Cai, Enhanced visible light photocatalytic activity of BiOCl by compositing with g-C_3N_4, Materials Research Innovations, 19 (2015) 392-396.

24. Q. Wang, W. Wang, L. Zhong, D. Liu, X. Cao, F. Cui, Oxygen vacancy-rich 2D/2D BiOCl-g-C_3N_4 ultrathin heterostructure nanosheets for enhanced visible-light-driven photocatalytic activity in environmental remediation, Applied Catalysis B: Environmental, 220 (2018) 290-302.
25. F. Chang, Y. Xie, J. Zhang, J. Chen, C. Li, J. Wang, X. Hu, Construction of exfoliated g-C_3N_4 nanosheets–BiOCl hybrids with enhanced photocatalytic performance, RSC Advances, 4 (2014) 28519-28528.
26. S. Kang, R. C. Pawar, C. S. Lee, Decoration of Au nanoparticles onto BiOCl sheets for enhanced photocatalytic performance under visible irradiation for the degradation of RhB dye, Journal of Experimental Nanoscience, 11 (2016) 853-871.
27. Q. Li, X. Zhao, J. Yang, C. J. Jia, Z. Jin, W. Fan, Exploring the effects of nanocrystal facet orientations in g-C_3N_4/BiOCl heterostructures on photocatalytic performance, Nanoscale, 7 (2015) 18971-18983.
28. Z. Cui, L. Mi, D. Zeng, Oriented attachment growth of BiOCl nanosheets with exposed {1 1 0} facets and photocatalytic activity of the hierarchical nanostructures, Journal of Alloys and Compounds, 549 (2013) 70-76.
29. G. Dong, L. Zhang, Porous structure dependent photoreactivity of graphitic carbon nitride under visible light, Journal of Materials Chemistry, 22 (2012) 1160-1166.
30. X. J. Wang, Q. Wang, F. T. Li, W. Y. Yang, Y. Zhao, Y. J. Hao, S. J. Liu, Novel BiOCl–C_3N_4 heterojunction photocatalysts: in situ preparation via an ionic-liquid-assisted solvent-thermal route and their visible-light photocatalytic activities, Chemical engineering journal, 234 (2013) 361-371.
31. P. Qiu, C. Xu, H. Chen, F. Jiang, X. Wang, R. Lu, X. Zhang, One step synthesis of oxygen doped porous graphitic carbon nitride with remarkable improvement of photo-oxidation activity: Role of oxygen on visible light photocatalytic activity, Applied Catalysis B: Environmental, 206 (2017) 319-327.
32. J. Wang, G. Zhang, J. Li, K. Wang, Novel three-dimensional flowerlike BiOBr/Bi_2SiO_5 p–n heterostructured nanocomposite for degradation of tetracycline: Enhanced visible light photocatalytic activity and mechanism, ACS Sustainable Chemistry & Engineering, 6 (2018) 14221-14229.
33. D. Monga, S. Basu, Enhanced photocatalytic degradation of industrial dye by g-C_3N_4/TiO_2 nanocomposite: Role of shape of TiO_2, Advanced Powder Technology, 30 (2019) 1089- 1098.

Thesis

ORIGINALITY REPORT

10%	2%	8%	5%
SIMILARITY INDEX	INTERNET SOURCES	PUBLICATIONS	STUDENT PAPERS

PRIMARY SOURCES

1	Qiao Wang, Wei Wang, Lingling Zhong, Dongmei Liu, Xingzhong Cao, Fuyi Cui. "Oxygen vacancy-rich 2D/2D BiOCl-g-C 3 N 4 ultrathin heterostructure nanosheets for enhanced visible-light-driven photocatalytic activity in environmental remediation", Applied Catalysis B: Environmental, 2018 Publication	2%
2	L. Cai. " Enhanced visible light photocatalytic activity of BiOCl by compositing with g-C N ", Materials Research Innovations, 2015 Publication	1%
3	Wee-Jun Ong, Lling-Lling Tan, Yun Hau Ng, Siek-Ting Yong, Siang-Piao Chai. " Graphitic Carbon Nitride (g-C N)-Based Photocatalysts for Artificial Photosynthesis and Environmental Remediation: Are We a Step Closer To Achieving Sustainability? ", Chemical Reviews, 2016 Publication	1%

Zhang, Shouwei, Jia-Xing Li, Xiangke Wang,

checked
23/07/19

4	Yongshun Huang, Meiyi Zeng, and Jinzhang Xu. "In-situ ion exchange synthesis of strongly coupled Ag@AgCl/g-C3N4 porous nanosheets as plasmonic photocatalyst for highly efficient visible-light photocatalysis", ACS Applied Materials & Interfaces Publication	1 %
5	Li, Qingbo, Xian Zhao, Jun Yang, Chun-Jiang Jia, Zhao Jin, and Weiliu Fan. "Exploring the effects of nanocrystal facet orientations in g-C3N4/BiOCl heterostructures on photocatalytic performance", Nanoscale, 2015. Publication	1 %
6	Submitted to Universiti Tunku Abdul Rahman Student Paper	1 %
7	clok.uclan.ac.uk Internet Source	1 %
8	dyuthi.cusat.ac.in Internet Source	1 %
9	Umar Ibrahim Gaya. "Heterogeneous Photocatalysis Using Inorganic Semiconductor Solids", Springer Nature, 2014 Publication	1 %
10	Seema Garg, Mohit Yadav, Amrish Chandra, Soniya Gahlawat, Pravin P. Ingole, Zsolt Pap, Klara Hernadi. "Plant leaf extracts as	<1 %